CrossMark

Theoretical and Experimental Study of Effective Shear Stiffness of Reinforced ECC Columns

Chang Wu[1], Zuanfeng Pan[2],* 🆔 **, Kang-Su Kim[3], and Shaoping Meng[4]**

Abstract: Engineered cementitious composites (ECC) possesses characteristics that make it suitable in the zones of high shear and ductility demand of structural elements; however, there is a lack of an adequate model to predict its shear stiffness. A theoretical model for the effective shear stiffness of reinforced ECC (RECC) columns is proposed on the basis of the truss-arch model, with the consideration of the unique property of ECC material. A total of six column specimens subjected to cyclic reverse loading are conducted, and the main test variables include the shear span-to-depth ratio, the transverse reinforcement ratio and the axial load ratio. Results show that the shear contribution to the total deflection in the diagonally cracked RECC beam is significant, and the proposed theoretical model can predict the shear deformation with reasonable accuracy.

Keywords: engineered cementitious composites (ECC), columns, experimentation, shear stiffness, truss, arch.

1. Introduction

Engineered cementitious composites (ECC) invented by Li et al. (Li 2012; Li and Leung 1992; Li et al. 1993) based on the basic principle of micromechanics and fracture mechanics is one of a family of high performance fiber reinforced cement composite (HPFRCC) (Naaman 1987), which exhibits pseudo strain hardening and multiple cracking properties under uniaxial tensile stress. This type of material consists of cement, mineral admixture, fine aggregates (maximum grain size usually 0.15 mm), water, admixtures to enhance strength and workability, and less than 2.0% volume of short fibers. Uniaxial tensile tests on ECC indicate that multiple fine cracks in ECC are formed uniformly over the length of the specimen, and the opening of each crack is usually less than 100 μm, subsequently, the ultimate tensile strain can exceed 2.0%, which is several hundred times that of normal concrete.

ECC has attracted the attentions of many researchers during the past two decades (Yoo and Yoon 2016), due to the advantages of unique macroscopic pseudo strain hardening,

high energy dissipation capacity and good durability. The randomly distributed fibers in ECC help to transfer loads at the internal micro cracks, which leads to the fact that RECC member can have a relatively higher load carrying capacity and deformation capacity compared to normal RC member. Generally, both ultimate strength limit state and serviceability limit state requirements should be considered in the structural design. As there is no coarse aggregate in ECC, the elastic modulus of ECC is usually lower than that of concrete. Consequently, greater deformation of RECC member tends to be caused. The design of RECC members may be controlled by the serviceability limit rather than strength. In addition, for seismic design, the stiffness of RECC members of a structure strongly influences the calculated response under seismic action. Therefore, it is important to accurately predict the effective stiffness up to yielding of each structural component. Generally, the total deformation of a structural member can be regarded as the summation of flexural and shear deformations. However, even for RC members, the shear mechanisms is not as clearly elucidated compared to the sound understanding of flexural behavior, and the shear deformation is usually underestimated or just neglected. For the newly developed material, ECC, few researches so far have been reported on the estimation of shear deformation of ECC members. To address this issue, an approach to predict the effective shear stiffness of RECC columns is proposed in the present study, based on the truss-arch model.

Since the truss concept was first introduced a century ago, the truss models have wildly used for predicting the ultimate shear strength of RC members, such as the traditional 45° truss model, constant angle truss model (CATM), variable angle truss model (VATM), compression field theory (CFT), modified compression field theory (MCFT), rotating-angle

[1]Department of Civil and Environmental Engineering, Hong Kong University of Science and Technology, Hong Kong, China.

[2]College of Civil Engineering, Tongji University, 200092 Shanghai, China.
*Corresponding Author; E-mail: zfpan@tongji.edu.cn
[3]Department of Architectural Engineering, University of Seoul, Seoul, Korea.
[4]School of Civil Engineering, Southeast University, 210096 Nanjing, China.

softened truss model (RA-STM) and fixed-angle softened truss model (FA-STM), etc. (ASCE-ACI Committee 445 1998). In terms of the study on shear stiffness or deformation, Kim and Mander (1999) systematically researched the truss model and analyzed the shear stiffness of RC columns with the VATM which was derived using various numerical integration schemes. The Programs, VecTor2 (Won and Vecchio 2002) and Response 2000 (Bentz 2000), were developed based on MCFT, which can be used to analyze the load–displacement curves of RC members subjected to the combination of axial load, shear and flexure. Based on Softened Membrane Model (SMM) (Hsu and Mo 2010), Mo et al. (2008) developed the Simulation of Concrete Structures (SCS) program on the OpenSEES platform to simulate the load–displacement responses of shear-critical RC elements. Pan et al. (2014) derived the explicit expression of effective shear stiffness on the basis of CATM and VATM, which was verified by the experiment of RC T-section beams.

In the truss-arch model, the shear resistant mechanism is explicitly considered as the truss action superimposing an arch action. Arch action in RC members subjected to shear force has been recognized by many researchers (Ichinose 1992; Kim et al. 1998). Especially, for members with low shear span-to-depth ratio, if the arch action is not taken into account, the shear stiffness tends to be underestimated. Ichinose (1992) presented a truss-arch model and proposed a design equation to prevent shear failure after the inelastic flexural deformation, which has been adopted in the Architectural Institute of Japan Design Guidelines (AIJ 1994). On the basis of the experimentally measured steel stresses over the shear span in the RC beams, Kim et al. (1998) proposed an empirical coefficient, which represents arch action contribution to the total shear capacity. Pan et al. (Pan and Li 2013; Jin and Pan 2015) proposed a new type of truss-arch model with the consideration of the deformation compatibility for both truss model and arch action, and the proposed model was verified by the shear-critical RC column tests.

The unique tensile strain-hardening property allows cracked ECC members to carry tensile stresses, and the tensile stress of cracked ECC can not be directly neglected like brittle materials such as normal concrete. In the present study, a theoretical model is proposed on the basis of the truss-arch model, incorporating the unique properties of ECC, to predict the effective shear stiffness of RECC columns. Then, six RECC columns subjected to cyclic reverse loading with various shear span-to-depth ratios, transverse reinforcement ratios and axial load ratios were studied experimentally to verify the proposed model.

2. Shear Stiffness for RECC Columns

2.1 Pre-cracking Shear Stiffness
As the applied shear force is less than the cracking shear force, V_{cr}, the member keeps diagonally uncracked and its shear behavior can be considered to be elastic. The shear stiffness before diagonally cracking, K_{v1}, can be calculated through elasticity method, as follows,

$$K_{v1} = GA_v = \frac{E_c A_v}{2(1 + \mu)} \approx 0.435 E_c A_v \qquad (1)$$

in which μ is the Poisson's ratio of ECC, and μ is equal to 0.15 (Han et al. 2003).

### 2.2 Truss-arch Model for Fully Diagonally Cracked Shear Stiffness
The truss-arch model method is employed to calculate the fully diagonally cracked shear stiffness of a RECC column in this study. Based on the truss-arch model, the fully diagonally cracked shear stiffness, K_{v2}, can be decoupled into two base components: the truss component, K_t, and the arch component, K_a. It can be calculated with the following equation:

$$K_{v2} = K_t + K_a \qquad (2)$$

In terms of the truss component, constant angle truss model (CATM) or variable angle truss model (VATM) can be employed to calculate the fully diagonally cracked shear stiffness, K_t, of a RECC column. It is well known that structural members can be divided into two standard regions, known as B-regions and D-regions (Schlaich et al. 1987), respectively. Bernoulli's hypothesis of plane strain distribution is assumed valid in B-regions, while the strain distribution along a section is disturbed in D-regions. The cracked shear stiffness in B-regions of a RECC column can be calculated by means of CATM, while VATM can be used in D-regions. In general, in a column with a high shear span-depth ratio, D-regions only exist near the concentrated loads and supports, while the other areas can be regarded as B-regions. In this case, a combined truss model (Fig. 1(a)) should be used to analyze the shear behavior of the column. However, the use of a combined truss model is relatively complicated. Pan et al. (2014) concluded that when the length of shear span $L_s > d_v \cot\theta_m$, the calculated shear stiffness using the CATM is close to the result calculated by the combined truss model. d_v represents the effective shear depth taken as flexural lever arm which need not be taken less than $0.9d$, θ_m is the minimum angle of the inclined strut. To simplify the analysis, only the CATM, instead of the combined truss model, is used to calculate the shear stiffness of a RECC column with a high shear span-depth ratio. For a column with a low shear span-depth ratio, the whole shear span area can be considered as D-regions, and VATM can be used to describe the shear behavior of the column (see Fig. 1(b)). The boundary that distinguishes the high and low shear span-depth ratio can be defined by the minimum inclined crack angle θ_m. Therefore, if the relationship $L_s > d_v \cot\theta_m$ is satisfied, the cracked shear stiffness of the column can be approximately calculated by the CATM; whereas if $L_s \leq d_v \cot\theta_m$, the VATM should be applied. The determination of the minimum inclined crack angle, θ_m, will be discussed later.

2.2.1 Shear Stiffness of CATM
The shear transfer mechanism of a RECC member in B-regions is revealed in Fig. 2(a). Generally, the inclined
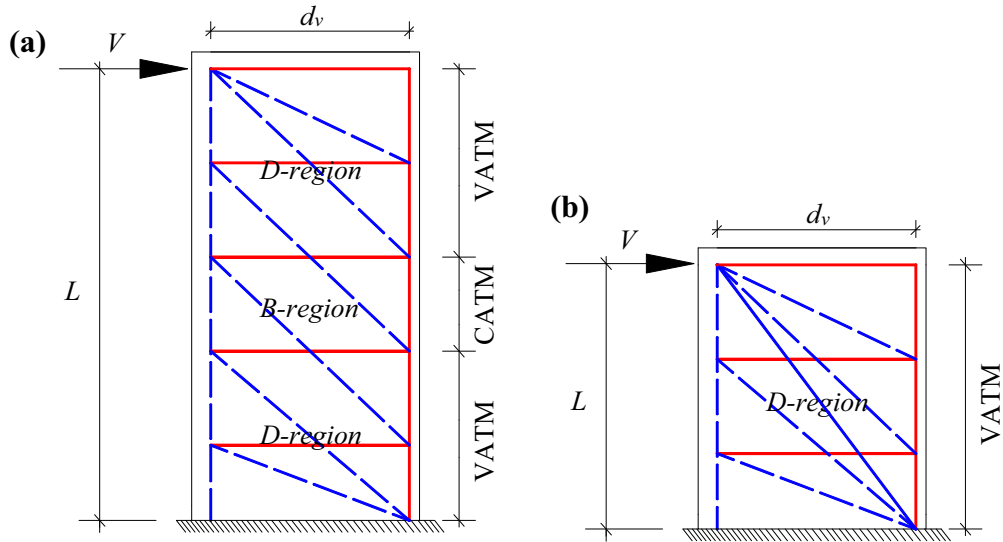
Fig. 1 Truss analogy modeling for RECC columns with different λ. **a** Combined truss model for high λ **b** VATM for low λ.

cracks in B-regions are approximately parallel. When inclined cracks develop, matrix between two adjacent inclined cracks carries compressive stress, which can be considered as a strut. In RC elements, ties in the truss model just consist of transverse reinforcements; but in RECC elements, the fiber bridging effect at the cracked interfaces can persistently carry tensile stresses. Hence, a combination of transverse reinforcements and fiber bridging effect at the cracks is considered as ties in the truss model for RECC columns.

Consider a differential truss in Fig. 2(b) subjected to a differential shear force dV_t, in which the in-plane width of the tie and strut are dx and $dx\sin\theta_0$, respectively. This differential truss can be expressed with the simplified diagram, as shown in Fig. 2(c). The member forces in the truss subjected to a unit shear force can be easily resolved by the static equilibrium, and the shear deformation of the differential truss subjected to dV_t can be analyzed based on the principles of virtual work. When calculating the shear deformation, the flexural deformation can be eliminated by assuming that the longitudinal chords (AB and CD in Fig. 2(c)) are very rigid. Therefore, only the strut BC and the tie BD are considered when calculating the shear deformation.

The rigidity of the strut BC in the differential truss model can be expressed as follows:

$$(EA)_{BC} = E_c bdx \, \sin\theta_0 \tag{3}$$

in which b and d are the width and effective depth of column, respectively.

With respect to the tie BD, the rigidity contributed by transverse reinforcements is expressed as follows:

$$(EA)_{BD,s} = \frac{E_s A_{sh} dx}{s} \tag{4}$$

in which A_{sh} is the cross section area of transverse reinforcement at spacing s.

While the rigidity contributed by the fiber bridging effect of the cracked ECC is assumed as follows:

$$(EA)_{BD,c} = \gamma E_c bdx \tag{5}$$

in which γ is the reduction factor of the rigidity for cracked ECC.

The reduction factor γ reflects the ratio of degraded rigidity (when the RECC member fully diagonally cracks) to uncracked rigidity, and is associated with the strain level around the cracks of ECC, and the greater the strain is the less the reduction factor is. Assuming that when the RECC member was fully diagonally cracked, the transverse reinforcement just yielded, the reduction factor γ can be then derived according to strain compatibility between steel and ECC as follows:

$$\gamma = n\frac{f_{cr}}{f_y} \tag{6}$$

in which f_{cr} and f_y are the crack strength of ECC and yield strength of reinforcing steel, respectively.

Therefore, the total rigidity of the tie BD is as follows:

$$(EA)_{BD} = \frac{E_s A_{sh} dx}{s} + \gamma E_c bdx = E_s \left(\frac{A_{sh}}{s} + \frac{\gamma b}{n}\right) dx \tag{7}$$

in which n equals to E_s/E_c.

The analysis process of the chord deformations using the principles of virtual work method is presented in Table 1. Thus, the shear deformation of the differential truss can be calculated with the following equation:

$$\Delta_t = \sum \frac{Ffl}{EA} = \frac{d_v dV_t}{E_c bdx}\left(\frac{1}{\sin^4\theta_0} + \frac{1}{\gamma + n\rho_v}\right) \tag{8}$$
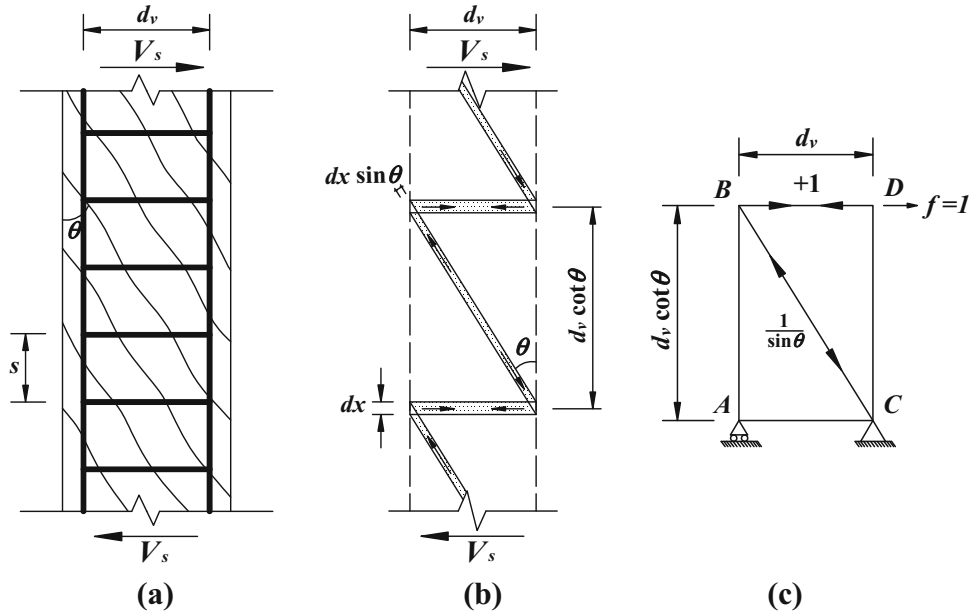
Fig. 2 Diagram of CATM.

in which ρ_v and f_y is the volumetric ratio of transverse reinforcement to concrete, $\rho_v = A_{sh}/(bs)$.

The corresponding rotation of the differential truss is as follows:

$$\theta_t = \frac{\Delta_t}{d_v \cot \theta_0} = \frac{dV_t}{E_c b \cot \theta_0 dx}\left(\frac{1}{\sin^4 \theta_0} + \frac{1}{\gamma + n\rho_v}\right) \quad (9)$$

Then, the differential shear stiffness of the differential truss can be written as:

$$dK_t = \frac{dV_t}{\theta_t} = \frac{E_c b \cot \theta_0 dx}{\frac{1}{\sin^4 \theta_0} + \frac{1}{\gamma + n\rho_v}} \quad (10)$$

The total shear stiffness of a cracked RECC member based on the CATM can be then derived by integrating Eq. (10) through the length of $d_v \cot \theta_0$,

$$K_t = \int_0^{d_v \cot \theta_0} dK_t = \frac{(\gamma + n\rho_v)\cot^2 \theta_0 E_c A_v}{1 + (\gamma + n\rho_v)\csc^4 \theta_0} \quad (11)$$

2.2.2 Shear Stiffness of VATM

A diagram of the shear transfer mechanism in D-regions for a short RECC column is shown in Fig. 3(a). It can be seen from Fig. 3(a) that the orientation of inclined cracks in D-regions are different and the cracks are idealized to intersect in the two diagonal corners. Consider a single differential truss, consisting of a tie with in-plane width of

Ldx (x ranges from 0 to 1) and two tapered struts with in-plane width tapered from $Ldx\sin\theta_1$ and $Ldx\sin\theta_2$ to 0 respectively, subjected to a differential shear force dV_t shown in Fig. 3(b). Similarly, the tie in the VATM for a RECC column also comprises the transverse reinforcements and the fiber bridging effect at the cracks. The tapered ECC strut can be idealized as a prismatic strut by averaging the in-plane width along the strut to simplify the calculation. This differential truss can be idealized as the simplified calculating diagram shown in Fig. 3(c). Assuming that the rigidity of the longitudinal chords in Fig. 3(c) are infinitely rigid, the shear deformation can be calculated by employing the principles of virtual work method. The analysis process of the chord deformations using the principles of virtual work method is given in Table 2.

The shear deformation of the differential truss can be calculated with the following equation:

$$\Delta_t = \sum \frac{Ffl}{EA} = \frac{d_v dV_t}{E_c A_v \cot \alpha dx}\left(2B + \frac{1}{\gamma + n\rho_v}\right) \quad (12)$$

in which, $B = [1 + x^2\cot^2\alpha]^2 + [1 + (1-x)^2\cot^2\alpha]^2$.

The corresponding rotation of the differential truss is as follows:

$$\theta_t = \frac{\Delta_t}{d_v \cot \alpha} = \frac{dV_t}{E_c A_v \cot^2 \alpha dx}\left(2B + \frac{1}{\gamma + n\rho_v}\right) \quad (13)$$

Then, the differential shear stiffness of the differential truss model can be written as:

Table 1 Chord deformations of CATM by the principles of virtual work method.

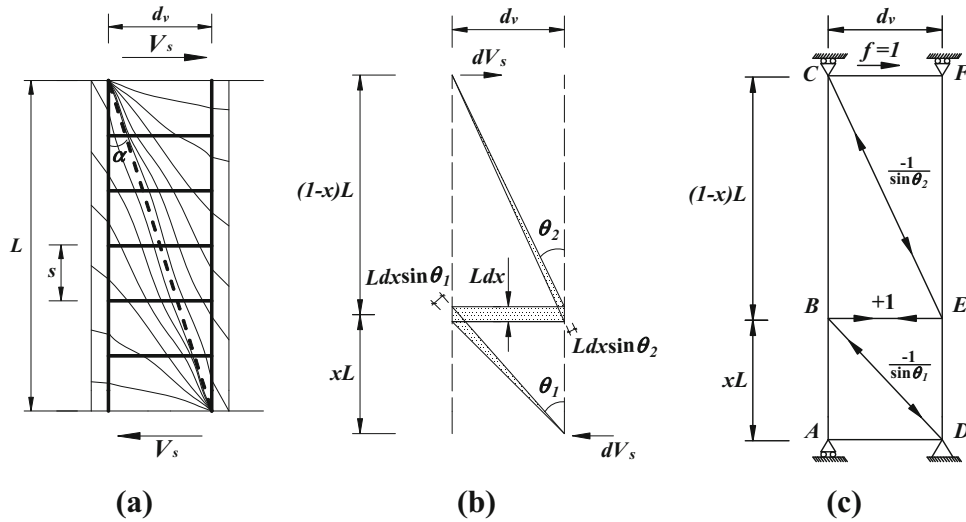| Member	Force	Unit load	Length	Rigidity	Deformation
	F	f	l	EA	Ffl/EA
BC	$-\frac{dV_t}{\sin\theta_0}$	$-\frac{1}{\sin\theta_0}$	$\frac{d_v}{\sin\theta_0}$	$E_c bdx \sin\theta_0$	$\frac{d_v dV_t}{E_c b \sin^4 \theta_0 dx}$
BD	$+ dV_t$	$+1$	d_v	$E_s\left(\frac{A_{sh}}{s} + \frac{b}{n}\right)dx$	$\frac{d_v dV_t}{E_s\left(\frac{A_{sh}}{s} + \frac{b}{n}\right)dx}$

Fig. 3 Diagram of VATM.

Table 2 Chord deformations of VATM by the principles of virtual work method.

Member	Force	Unit load	Length	Rigidity	Deformation
	F	f	l	EA	Ffl/EA
BD	$-\dfrac{dV_t}{\sin\theta_1}$	$-\dfrac{1}{\sin\theta_1}$	$\dfrac{d_v}{\sin\theta_1}$	$\dfrac{E_c bL \sin\theta_1 dx}{2}$	$\dfrac{2d_v dV_t}{E_c bL \sin^4\theta_1 dx}$
CE	$-\dfrac{dV_t}{\sin\theta_2}$	$-\dfrac{1}{\sin\theta_2}$	$\dfrac{d_v}{\sin\theta_2}$	$\dfrac{E_c bL \sin\theta_2 dx}{2}$	$\dfrac{2d_v dV_t}{E_c bL \sin^4\theta_2 dx}$
BE	$+ dV_t$	$+1$	d_v	$E_s\left(\dfrac{A_{sh}}{s}+\dfrac{b}{n}\right)Ldx$	$\dfrac{d_v dV_t}{E_s\left(\frac{A_{sh}}{s}+\frac{b}{n}\right)Ldx}$

$$dK_t = \frac{dV_t}{\theta_t}$$
$$= \frac{E_c A_v \cot^2\alpha\, dx}{2\left\{[1 + x^2\cot^2\alpha]^2 + \left[1 + (1-x)^2\cot^2\alpha\right]^2\right\} + \frac{1}{\gamma + n\rho_v}} \tag{14}$$

By integrating Eq. (14) from 0 to 1, the total shear stiffness of a cracked RECC member based on VATM can be then derived as:

$$K_t = \int_0^1 dK_t$$
$$= \int_0^1 \frac{E_c A_v \cot^2\alpha}{2\left\{[1 + x^2\cot^2\alpha]^2 + \left[1 + (1-x)^2\cot^2\alpha\right]^2\right\} + \frac{1}{\gamma + n\rho_v}} dx \tag{15}$$

It's worth noting that a closed-form solution can be hardly obtained from the Eq. (15). Kim and Mander (1999) provided several numerical solutions for shear stiffness of VATM using different numerical integration methods, including Two-point Gauss, Three-point Gauss, et al. By comparing the results analyzed by different methods, it can be concluded that the results are reasonably close. Since the two-point Gauss integration method can provide the simplest form of solution with sufficient accuracy, it is selected as the tool to derive the post-cracking shear stiffness of VATM in

this study. Using the two-point Gauss integration method, the shear stiffness of VATM can be derived as:

$$K_t = \frac{(\gamma + n\rho_v)E_c A_v \cot^2\alpha}{1 + 2(\gamma + n\rho_v)\left\{[1 + 0.04\cot^2\alpha]^2 + [1 + 0.62\cot^2\alpha]^2\right\}} \tag{16}$$

Equation (16) can be further simplified to the following equation:

$$K_t = \frac{(\gamma + n\rho_v)\cot^2\alpha\, E_c A_v}{1 + 4(\gamma + n\rho_v)(1 + 0.39\cot^2\alpha)^2} \tag{17}$$

2.2.3 Shear Stiffness of Arch Component

The arch component is assumed as a single compressive strut directed from the compression zone at the top toward that at the bottom (see Fig. 4). If the column is in double bending, the inclination of the strut is found from the line joining the centers of flexural compression at the top and at the bottom of the column (Fig. 4(a)). If the column is constrained with fixed-pinned ends, the inclination of the strut is formed at the axis at the top and the center of flexural compression at the bottom of the column (Fig. 4(b)). In the arch model, the shear deformation is induced by the compression of the strut (Fig. 4(a)). The width of the arch strut is $c_a\cos\alpha$, where c_a is the effective depth of the strut in the arch model. And conservatively, effective depth c_a is expressed as
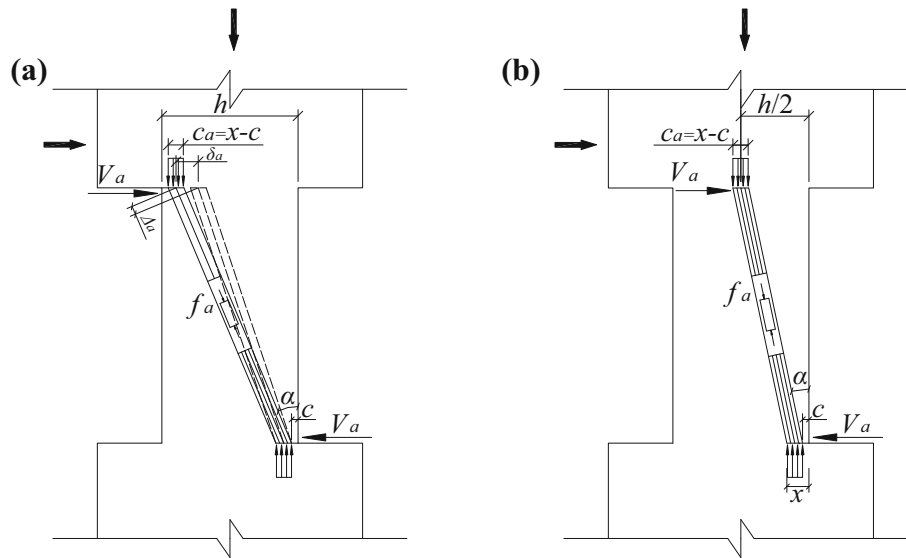
Fig. 4 Diagram of arch action. **a** column with fixed–fixed ends **b** column with fixed pinned ends.

$c_a = x - c$, where x is the depth of compressive zone and c is the thickness of ECC cover. The shear stiffness of the arch model (Pan and Li 2013) can be calculated with the following equation:

$$K_a = E_c b c_a \sin^2 \theta_a \cos^2 \theta_a \tag{18}$$

in which θ_a is the inclination of the strut for a column with fixed–fixed ends (Fig. 4(a), $\theta_a = \mathrm{atan}((h-x)/L)$) and for a column with fixed-pinned ends (Fig. 4(b), $\theta_a = \mathrm{atan}((h-x)/(2L))$). The depth of compressive zone, x, can be estimated by the following equation proposed by Paulay and Priestley (1992) for RC members,

$$x = \left(0.25 + 0.85 \frac{N}{f'_c A_g}\right) h \tag{19}$$

It is worth noting that the ECC material can carry tensile stress in the tension zone, which may cause greater depth of compressive zone, compared with the normal concrete. The method for predicting the depth of compressive zone of ECC members has not been well studied in resent researches. Here, the existing equation for RC members is used for simplicity and conservation. Theoretically, to balance the sectional tensile force, and therefore, the stiffness due to arch action will increase, while the predicted shear deformation will decrease.

2.2.4 Determination of the Minimum Inclined Crack Angle

As discussed above, the employment of CATM or VATM for analyzing the shear stiffness should be determined based on the minimum inclined angle θ_m. The cotangent of minimum inclined angle, $\cot\theta_m$, represents the critical aspect ratio to utilize CATM; when the aspect ratio is less than $\cot\theta_m$, the VATM should be applied. To determine the minimum inclined angle, a simplified truss model with two-point Gauss quadrature can be used, shown as Fig. 5. It is

believed that the minimum inclined crack angle depends on both flexure and shear components, and will occur at an inclination that requires the minimum potential energy.

Assuming the truss shown in Fig. 5 is subjected to a unit shear force, the external work done, EWD, can be written as the total drift angle of flexure and shear components,

$$\mathrm{EWD} = \theta_f + \theta_s \tag{20}$$

As mentioned above, the shear rotation can be obtained as follows,

$$\theta_s = \frac{1}{K_t} = \frac{1 + 4(\gamma + n\rho_v)(1 + 0.39 \cot^2 \alpha)^2}{(\gamma + n\rho_v) \cot^2 \alpha E_c A_v} \tag{21}$$

The flexural rotation can be induced by the deformations of the longitudinal chords in Fig. 5. Assuming that the sectional depth ratio of compression zone of ECC members is ξ, and the sectional depth ratio of tension zone equals to $(1-\xi)$. The rigidity of the chords in tension (AB,
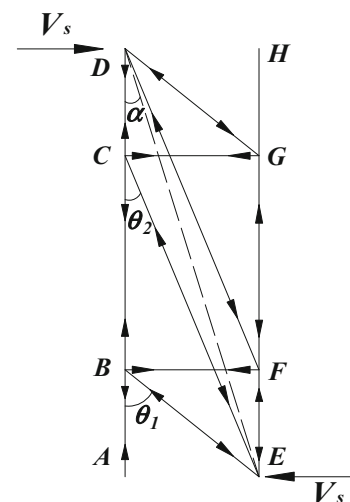
Fig. 5 Variable angle truss model by two-point Gauss quadrature.

Table 3 Chord deformations of VATM by two-point Gauss quadrature.

Member	Force F	Unit load f	Length l	Rigidity EA	Deformation Ffl/EA
AB	$\cot\alpha$	$\cot\alpha$	$x_1 L$	$E_s\left[\frac{A_{st}}{2}+\frac{\gamma(1-\xi)bh}{n}\right]$	$\frac{x_1 L\cot^2\alpha}{E_s\left[\frac{A_{st}}{2}+\frac{\gamma(1-\xi)bh}{n}\right]}$
BC	$(2-x_1)\cot\alpha/2$	$(2-x_1)\cot\alpha/2$	$(1-2x_1)L$	$E_s\left[\frac{A_{st}}{2}+\frac{\gamma(1-\xi)bh}{n}\right]$	$\frac{L\cot^2\alpha(1-x_1)^2(1-2x_1)}{4E_s\left[\frac{A_{st}}{2}+\frac{\gamma(1-\xi)bh}{n}\right]}$
CD	$\cot\alpha/2$	$\cot\alpha/2$	$x_1 L$	$E_s\left[\frac{A_{st}}{2}+\frac{\gamma(1-\xi)bh}{n}\right]$	$\frac{x_1 L\cot^2\alpha}{4E_s\left[\frac{A_{st}}{2}+\frac{\gamma(1-\xi)bh}{n}\right]}$
EF	$-\cot\alpha/2$	$-\cot\alpha/2$	$x_1 L$	$E_s\left(\frac{A_{st}}{2}+\frac{\xi bh}{n}\right)$	$\frac{x_1 L\cot^2\alpha}{4E_s\left(\frac{A_{st}}{2}+\frac{\xi bh}{n}\right)}$
FG	$-x_1\cot\alpha/2$	$-x_1\cot\alpha/2$	$(1-2x_1)L$	$E_s\left(\frac{A_{st}}{2}+\frac{\xi bh}{n}\right)$	$\frac{x_1^2(1-2x_1)L\cot^2\alpha}{4E_s\left(\frac{A_{st}}{2}+\frac{\xi bh}{n}\right)}$
GH	0	0	$x_1 L$	$E_s\left(\frac{A_{st}}{2}+\frac{\xi bh}{n}\right)$	0

Note $x_1 = 0.21$.

BC, and CD in Fig. 5) consists of axial stiffness contributed by reinforcements and fiber bridging effects of the cracked ECC, which can be written as,

$$(EA)_{tens} = \frac{E_s A_{st}}{2} + \frac{\gamma E_s(1-\xi)bh}{n} \qquad (22)$$

Generally, the longitudinal reinforcements in columns are symmetric about the centroidal axis; therefore, $A_{st}/2$ is applied in Eq. (22), in which A_{st} is the total area of the longitudinal reinforcement.

While, the rigidity of the chords in compression (EF, FG, and GH in Fig. 5) can be expressed as,

$$(EA)_{comp} = \frac{E_s A_{st}}{2} + \frac{E_s \xi bh}{n} \qquad (23)$$

Since no test has been conducted to determine the sectional depth of compression zone for RECC members, the sectional depth ratio of compression zone, ξ, can be estimated by the following equation (Paulay and Priestley 1992),

$$\xi = \frac{x}{h} = 0.25 + 0.85\frac{N}{f_c' A_g} \qquad (24)$$

If the VATM with two-point Gauss quadrature shown in Fig. 5 is subjected to a unit shear force, the deformations of each chord are listed in Table 3. Then, the flexural drift angle can be calculated as follows,

$$\theta_f = \frac{\Delta_f}{L} = \frac{\cot^2\alpha}{E_c A_g}\left(\frac{1.46}{n\rho_s + 2\gamma(1-\xi)} + \frac{0.12}{n\rho_s + 2\xi}\right) \qquad (25)$$

Therefore, the external work done, EWD, can be written as the total drift angle of Eq. (21) and (25),

$$EWD = \frac{1 + 4(\gamma + n\rho_v)(1 + 0.39\cot^2\alpha)^2}{(\gamma + n\rho_v)\cot^2\alpha E_c A_v}$$
$$+ \frac{\cot^2\alpha}{E_c A_g}\left(\frac{1.46}{n\rho_s + 2\gamma(1-\xi)} + \frac{0.12}{n\rho_s + 2\xi}\right) \qquad (26)$$

Letting $\alpha = \theta_m$, and $dEWD/d\theta_m = 0$, the minimum inclined angle θ_m can be then derived as,

$$\theta_m = \arctan\left[\left(\frac{0.61 + \frac{A_v}{A_g}\left(\frac{1.46}{n\rho_s + 2\gamma(1-\xi)} + \frac{0.12}{n\rho_s + 2\xi}\right)}{4 + \frac{1}{n\rho_v + \gamma}}\right)^{\frac{1}{4}}\right] \qquad (27)$$

2.2.5 Determination of Constant Crack Angle

It can be seen from Eq. (11) that the constant crack angle θ_0 is the only unknown variable to obtain the shear stiffness of the CATM. In this study, the constant crack angle θ_0 is also derived based on the principle of minimum energy. By replacing the shear drift angle, θ_s, in Eq. (26) with Eq. (9) deduced by the CATM, and letting $\alpha = \theta_0$, the external work done, EWD, can be expressed as,

$$EWD = \frac{1 + (\gamma + n\rho_v)\csc^4\theta_0}{(\gamma + n\rho_v)\cot^2\theta_0 E_c A_v} + \frac{\cot^2\theta_0}{E_c A_g}$$
$$\left(\frac{1.46}{n\rho_s + 2\gamma(1-\xi)} + \frac{0.12}{n\rho_s + 2\xi}\right) \qquad (28)$$

By differentiating Eq. (28) with respect to θ_0, and letting the result equals to zero to minimize the external work done, the constant crack angle θ_0 can be derived as,

$$\theta_0 = \arctan\left[\left(\frac{1 + \frac{A_v}{A_g}\left(\frac{1.46}{n\rho_s + 2\gamma(1-\xi)} + \frac{0.12}{n\rho_s + 2\xi}\right)}{1 + \frac{1}{n\rho_v + \gamma}}\right)^{\frac{1}{4}}\right] \qquad (29)$$

2.3 Post-cracking Effective Shear Stiffness

A typical shear force—deformation response of a RECC column before yielding is shown in Fig. 6. The RECC column first cracks diagonally when the shear force reaches V_{cr}, at which the principal tensile stress in a RECC element reaches the tensile strength of ECC. Then, the shear stiffness drops suddenly due to the occurrence of first inclined crack; and as shear force increases, more inclined cracks form, which leads to the decease of shear stiffness of the RECC column. The actual response after cracking is shown as the curved line AB in Fig. 6. To simplify the calculation for the effective shear stiffness, the actual shear force–deformation

curve (line AB) can be idealized as the straight solid line AC (Fig. 6). Assuming the shear stiffness is K_{v2} when the column is fully cracked diagonally, thus, the slope of line AC can be written as follows:

$$K_{AC} = \frac{V_y - V_{cr}}{\frac{V_y}{K_{v2}} - \frac{V_{cr}}{K_{v1}}} \qquad (30)$$

The effective shear stiffness between K_{v1} and K_{v2} (the slope of the line OP in Fig. 6, and P is an arbitrary point along line AC) can be further obtained by using the linear interpolation as follows:

$$K_{veff} = \frac{V}{\frac{V_{cr}}{K_{v1}} + \frac{V - V_{cr}}{K_{AC}}} = \frac{V}{\frac{V_{cr}}{K_{v1}} + \frac{V - V_{cr}}{V_y - V_{cr}}\left(\frac{V_y}{K_{v2}} - \frac{V_{cr}}{K_{v1}}\right)} \qquad (31)$$

The calculation procedure can be expressed as the flow chart as shown in Fig. 7.

3. Experimental Program

3.1 Specimens and Material Properties

Six RECC columns, referred to as Specimens E1 $\sim$ E6, were tested in this experimental program. All columns had the same cross section of 300×300 mm. The heights of prepared columns were 500, 600 and 900 mm, and the corresponding shear span-to-depth ratios were 1.42, 1.75 and 2.75, respectively. The longitudinal reinforcement ratio was a constant of 1.4% for all specimens. The transverse reinforcement ratio ρ_{sv} was equal to 0.22% for E5 and E6 did not contain stirrups, while ρ_{sv} was 0.45% for the others. The applied axial compression for Specimen E4 was 700 kN, while it was 350 kN for the others. The detailed information of specimens is shown in Fig. 8 and Table 4.

The mix proportion of ECC material employed in this study was based on a high volume of fly ash (the weight ratio of fly ash to cement is 3.2) and 2.0% PVA fiber in volume fraction. Based on the tensile uniaxial test results (Pan et al. 2015), the PVA-ECC materials employed in this study had the tensile strength ranging from 4 MPa to 4.5 MPa, and the ultimate tensile strain was ranging from 4.0 to 5.0% at 28 days. A number of ECC cubes ($100 \times 100 \times 100$ mm) and prisms
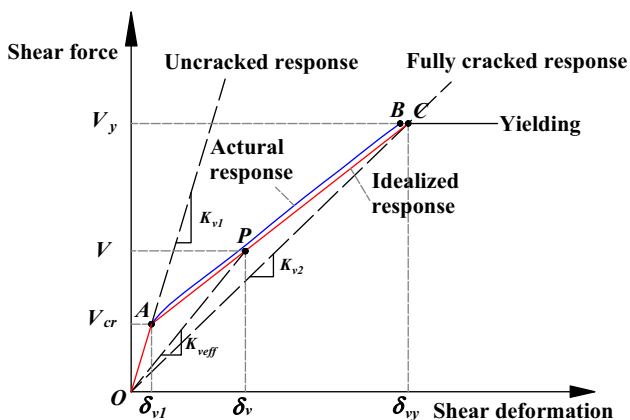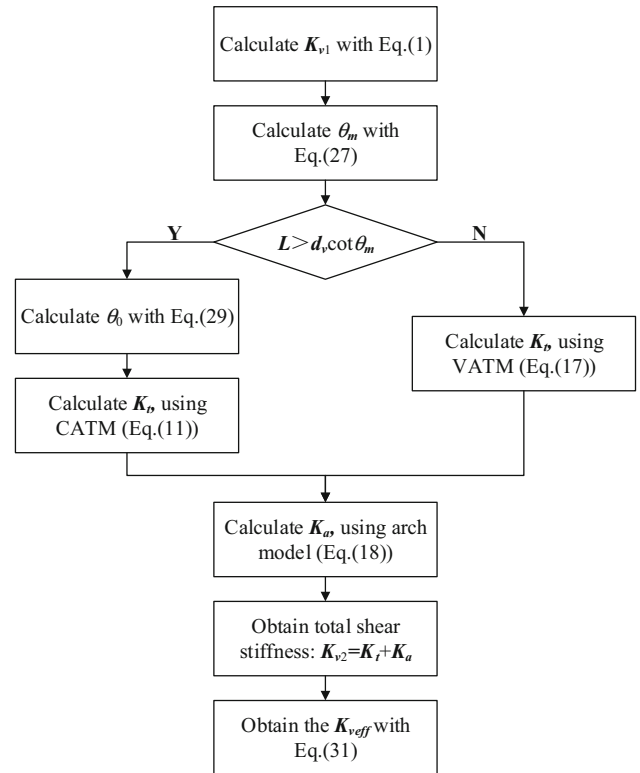
Fig. 7 Flowchart showing solution algorithm for effective shear stiffness.

($100 \times 100 \times 300$ mm) were also prepared and tested in compression. The tested average cubic compressive strength of prepared ECC was about 50 MPa, and the corresponding prismatic compressive strength was approximately 45 MPa. The elastic modulus of prepared ECC was about 22GPa. The detailed material properties are listed in Table 5.

The longitudinal steel bars employed in each specimen were four 20 mm-diameter deformed bars with a yield stress of 498 MPa. The stirrups used with the specimens were 8 mm-diameter deformed bars with a yield stress of 408 MPa.

3.2 Test Setup and Loading Configuration

The base mat of each specimen was fully fixed, while the top of the specimen was free to move horizontally. The transverse load was applied at the top of the column through a double-action actuator (with force and displacement control system) with a load capacity of 1000 kN fixed on a reaction wall. The axial load was applied on the centroid of the free end section of the specimen through a 1000 kN hydraulic jack keeping constant throughout the test. During the test, displacements were measured by means of linear variable differential transducers (LVDTs), while strains of reinforcement were measured by means of strain gauges. The location of strain gauges can be found in Fig. 8. The axial load was first applied to the target value and maintained constant by adjusting the readings of instrument panel in the hydraulic jack during the experiment. In the tests, a force-control loading program was applied before the longitudinal reinforcement yielded. The increment of load was initially
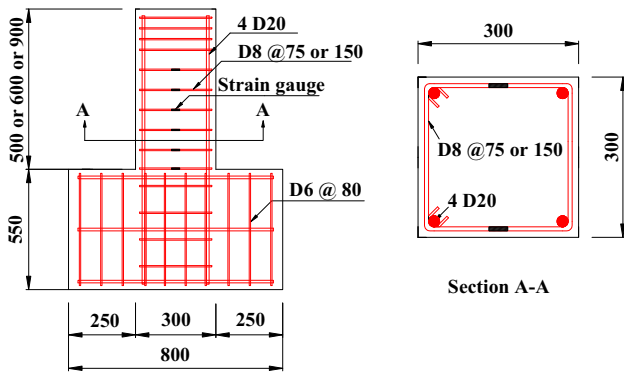
Fig. 6 Diagram of effective shear stiffness of RECC columns.

Fig. 8 Geometry and reinforcement details (unit: mm).

50 kN for each step until arriving at 80% of the predicted yielding load, and then changed the increment of 50 kN into 25 kN. The force-control loading procedure was not changed until the longitudinal reinforcement yielded. Then, the specimens were subjected to the cyclic shear force by the displacement-control loading method with the increment of each load step equals to the measured yield displacement up until the shear-resisting capacity drops by more than 20% of the maximum shear force. In the force-control loading procedure, all cycles were carried out once, while each displacement level was repeated three times in the displacement-control loading procedure. The detailed experiment setup and loading configuration can be found in the experimental study of ECC columns by Wu et al. (2017).

4. Discussion of Test and Predicted Results

4.1 Crack Patterns and Failure Modes

When the columns failed, main inclined cracks can be only observed in Specimen E1 which failed by flexure-shear mode, while others failed by flexure. The crack patterns at failure are shown in Fig. 9. From Eq. (27), the CATM was selected to analyze the shear behavior of all the tested columns. It is in accord with the observation, since most of the inclined cracks were almost parallel to each other in all the columns as shown in Fig. 9. The measured V_{cr}, V_y, and averaged crack angle θ_{avg} for the tested columns are shown in Table 6, along with the predicted crack angle θ_{pre} by Eq. (29). After testing, the averaged crack angle θ_{avg} is obtained by averaging the measured inclined angles of main diagonal cracks corresponding to the loading direction in which the specimen failed at loading moment. The failure point in the backbone curve is defined as the point at which the lateral force falls by more than 20% of the maximum shear force, and then the experiment ends. It is evident that the predicted crack angles using Eq. (29) are in agreement with the averaged experimentally observed crack angles. Moreover, Eq. (29) reveals that the inclined crack angle of a RECC column is dependent on the amount of longitudinal and transverse reinforcement, as well as the fiber bridging effect.

4.2 Deformation Comparison

To validate the proposed model for calculating the effective shear stiffness, the total displacements before yielding of six tested columns, consisting of flexural and shear deformation, were calculated and compared with the measured data as shown in Fig. 10. In Fig. 10, the test data "left" and "right" mean the data obtained in the negative and positive loading direction, respectively. The flexural displacement, δ_f, was obtained by translating the nonlinear moment–curvature relationship calculated by the strip method into the load–displacement curve. The shear deformation, δ_s, was obtained by $\delta_s = V/K_{veff}$, in which the effective shear stiffness K_{veff} is calculated by Eq. (3). It's worth noting that the measured V_{cr} and V_y were used directly in calculating K_{veff}. It can be seen from Fig. 10 that the calculated flexural deformations are obviously less than the measured deformations, except for Specimen E3, which has the highest shear span-to-depth ratios ($\lambda = 2.75$). After the columns were cracked diagonally, the difference increases significantly between the calculated flexural deformations and the measured total deformations of the columns with lower shear span-to-depth ratios, which indicates that the continuously developed cracks cause the increase of shear deformation in those columns. By combining the shear deformation δ_s calculated

Table 4 Summary of specimen information.

Specimen	λ	P (kN)	ρ_{sv} (%)
E1	1.42	350	0.45
E2	1.75	350	0.45
E3	2.75	350	0.45
E4	1.75	700	0.45
E5	1.75	350	0.22
E6	1.75	350	0

Table 5 Properties of ECC.

Material	f_{cu} (MPa)	f_c (MPa)	f_t (MPa)	ε_t (%)	E (GPa)
ECC	49.7	45.0	4.39	4.46	22.2
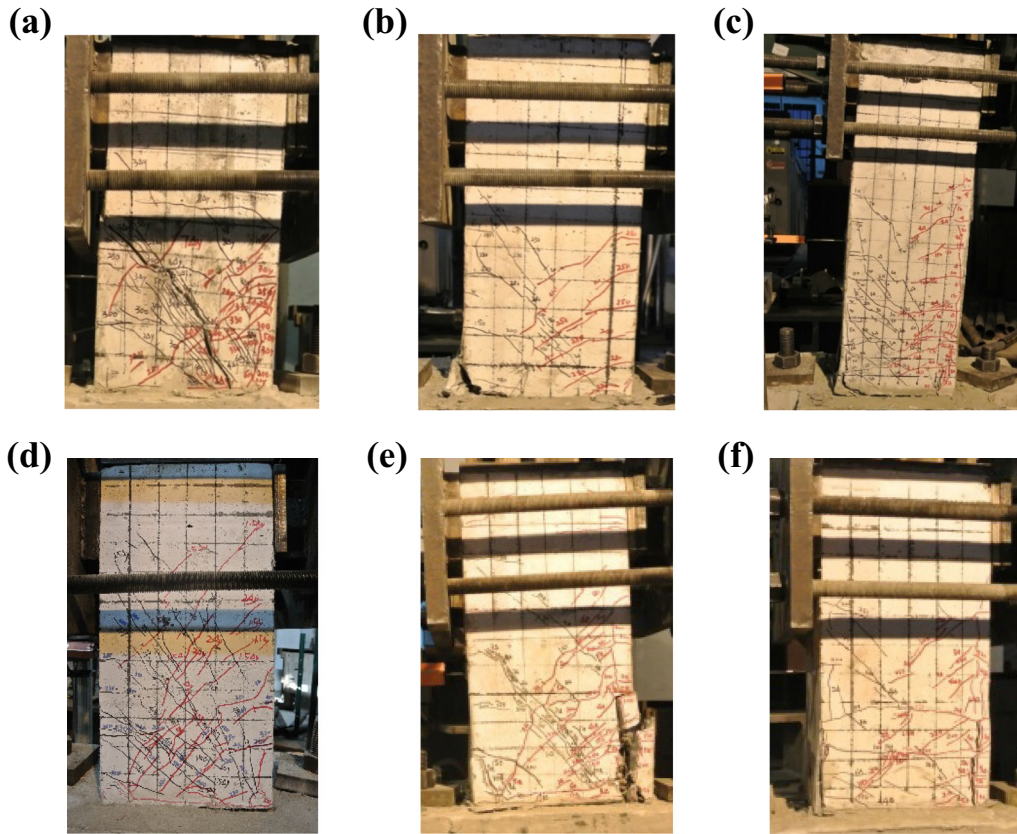
Fig. 9 Crack patterns of specimens at failure. **a** Specimen E1, **b** Specimen E2, **c** Specimen E3, **d** Specimen E4, **e** Specimen E5 and **f** Specimen E6.

Table 6 Summary of experimental and predicted results.

Specimen	V_{cr} (kN)	V_y (kN)	δ_y (mm)	θ_{avg} (°)	θ_{pre} (°)	δ_{pre} (mm)
E1	200	− 330.05	− 1.84	40	42.5	1.91
		330.12	1.92			
E2	150	− 280.00	− 3.02	42	42.5	2.90
		279.91	3.02			
E3	75	− 165.24	− 3.68	45	42.5	4.11
		165.92	3.60			
E4	200	− 382.09	− 3.09	42	42.8	2.89
		380.80	2.84			
E5	100	− 202.47	− 2.56	41	41.2	2.54
		240.16	2.35			
E6	100	− 196.58	− 2.50	40	39.4	2.26
		216.24	2.60			

Note The negative value represents the data obtained at the negative loading direction.

by the proposed approach, the calculated load–displacement curves, with respect to the total displacement ($\delta_f + \delta_s$), are in good agreement with the measured responses. The predicted displacement at yielding for Specimen E3 is slightly greater than the measured data. This is because the Specimen E3 has the greatest shear span-to-depth ratio, and consequently the shear contribution to the total deformation was relatively small compared to the flexural contribution. The comparison of measured and calculated deformation at yielding is shown in Table 6.
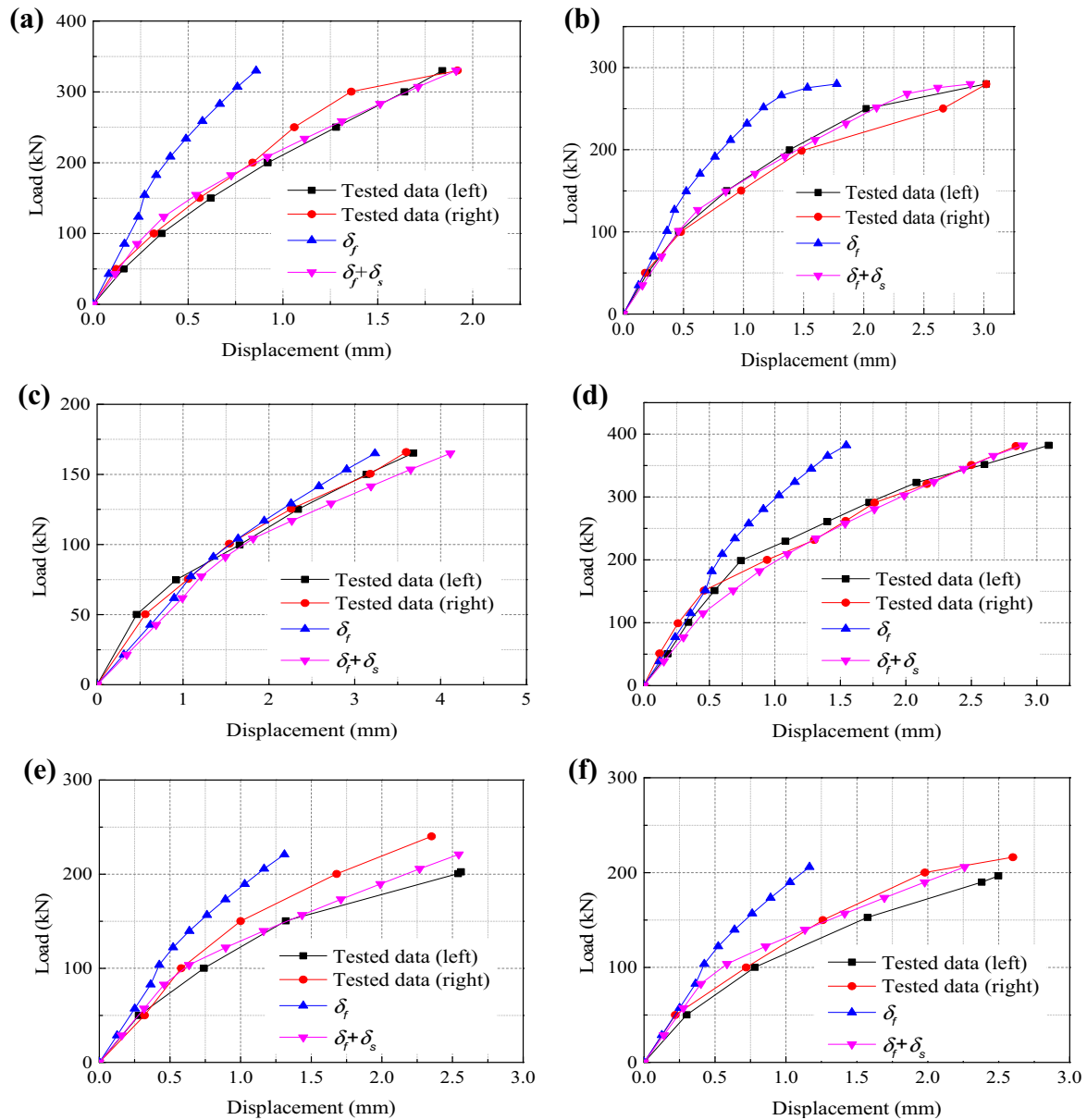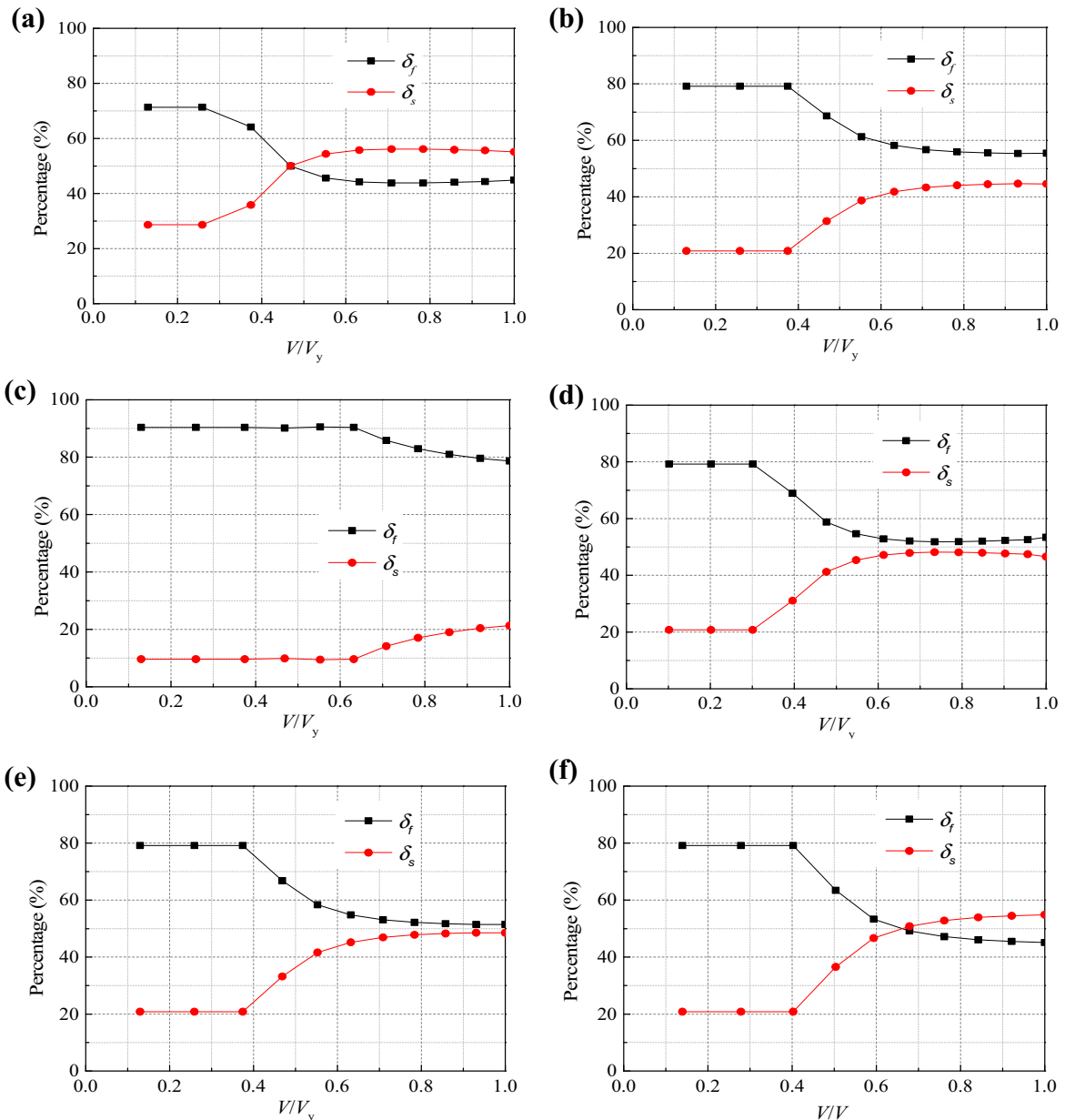
Fig. 10 Measured and predicted load–displacement curves of RECC columns. **a** Specimen E1, **b** Specimen E2, **c** Specimen E3, **d** Specimen E4, **e** Specimen E5 and **f** Specimen E6.

4.3 Proportion of Flexural and Shear Deformation

The percentages of flexural and shear deformations of each RECC column varied with the ratio V/V_y are shown in Fig. 11. It can be seen from Fig. 11 that the flexural deformations are greater than the related shear deformations for all specimens before diagonally cracking. With the development of inclined cracks, the proportion of shear deformation increases, and gradually becomes stable. The proportions of flexural and shear deformations vary with the different shear span-to-depth ratios. The proportion of shear deformation decreases with the increase of shear span-to-depth ratio, and on the contrary, the proportion of flexural deformation increases. For instance, Specimen E3 with the highest shear span-to-depth ratio ($\lambda = 2.75$), the proportion of flexural deformation exceeds 90% before diagonally cracking; even if the inclined cracks have fully developed,

the increase rate of shear deformation is much lower than the other specimens and the percentage of flexural deformation reduces to around 80%. Compared to Specimen E3, the increase of shear deformation of Specimen E1 is more significant, and when the load level reaches over $0.5V_y$, the percentage of shear deformation goes beyond 50%. Comparing the specimens with different transverse reinforcement ratios, E2 ($\rho_{sv} = 0.45\%$), E5 ($\rho_{sv} = 0.22\%$) and E6 ($\rho_{sv} = 0$), it can be concluded that the percentage of shear deformation reduces with the increasing transverse reinforcement ratio. For Specimen E6, the percentage of shear deformation even surpasses that of flexural deformation when the shear force reaches a certain level after diagonally cracking. It is evident that shear contribution to the total deformation for the diagonally cracked RECC columns is significant, especially for the RECC columns with low shear span-to-depth ratios.

Fig. 11 Percentage of flexural and shear deformations before yielding of RECC columns. **a** Specimen E1, **b** Specimen E2, **c** Specimen E3, **d** Specimen E4, **e** Specimen E5 and **f** Specimen E6.

5. Conclusions

A theoretical model for the effective shear stiffness of RECC columns is proposed based on the truss-arch model in this study. From the results of the experimental observation and the comparison between the tested and predicted, the following conclusions can be drawn:

1. By assuming that the load–displacement response of RECC column from the first cracking diagonally to the yielding is linear, the effective shear stiffness between the elastic shear stiffness and fully diagonally cracking shear stiffness is derived using the linear interpolation method.

2. Based on the truss-arch model, the fully diagonally cracked shear stiffness is considered as the combination of a truss component and an arch component. For the truss component, explicit formulas for calculating the fully diagonally cracked shear stiffness based on CATM and VATM were provided, respectively. The selection of truss model used is determined by the minimum crack angle which was obtained through the principle of minimum potential energy. In view of the tensile strain-hardening behavior of ECC material, the ties in the truss model for RECC columns were proposed to be consisted of the transverse reinforcement and the fiber bridging effect at cracks.

3. Six RECC columns with various shear span-to-depth ratios, transverse reinforcement ratios and axial loads were studied experimentally to verify the proposed model. Comparison of the measured and calculated deformation of RECC columns indicate that the observed and calculated crack angles are comparable,

and the theoretical results using the proposed model of effective shear stiffness are shown to be consistent with the shear behavior observed experimentally. By analyzing the proportion of shear and flexural deformation, it can be concluded that the shear contribution to the total deformation for the diagonally cracked RECC column is significant, especially for the RECC columns with low shear span-to-depth ratios.

Open Access

References

Architectural Institute of Japan (AIJ). (1994). *AIJ structural design guidelines for reinforced concrete buildings*, Tokyo.

ASCE-ACI Committee 445. (1998). Recent approaches on shear design of structural concrete. *Journal of Structural Engineering, 124*(12), 1375–1417.

Bentz, E. C. (2000). *Sectional analysis of RC members*. Ph.D. thesis, Canada: University of Toronto.

Han, T. S., Feenstra, P. H., & Billington, S. L. (2003). Simulation of highly ductile fiber-reinforced cement-based composite components under cyclic loading. *ACI Structural Journal, 100*(6), 749–757.

Hsu, T. T. C., & Mo, Y. L. (2010). *Unified theory of reinforced concrete*. Hoboken, New Jersey: John Wiley & Sons Ltd.

Ichinose, T. (1992). A shear design equation for ductile RC members. *Earthquake Engineering and Structural Dynamics, 21*(3), 197–214.

Jin, C., Pan, Z., Meng, S., & Qiao, Z. (2015). Seismic behavior of shear-critical reinforced high-strength concrete columns. *Journal of Structural Engineering, 141*(8), 04014198.

Kim, D. J., Kim, W., & White, R. N. (1998). Prediction of reinforcement tension produced by arch action in RC beams. *Journal of Structural Engineering, 124*(6), 611–622.

Kim, J. H. & Mander, J. B. (1999). Truss modeling of reinforced concrete shear-flexure behavior. Technical report MCEER-99-0005. New York: Multidisciplinary center for earthquake engineering research, State University of New York at Buffalo, New York.

Li, V. C. (2012). Tailoring ECC for special attributes: a review. *International Journal of Concrete Structures and Materials, 6*(3), 135–144.

Li, V. C., & Leung, C. K. Y. (1992). Steady state and multiple cracking of short random fiber composites. *Journal of Engineering Mechanics, 188*(11), 2246–2264.

Li, V. C., Stang, H., & Krenchel, H. (1993). Micromechanics of crack bridging in fiber reinforced concrete. *Materials and Structure, 26*(162), 486–494.

Mo, Y. L., Zhong, J., & Hsu, T. T. C. (2008). Seismic simulation of RC wall-type structures. *Engineering Structures, 30*(11), 3167–3175.

Naaman, A. E. (1987). High performance fiber reinforced cement composites. In *Proceedings of the IABSE symposium on concrete structures for the future, Paris, France* (pp. 371–376).

Pan, Z., & Li, B. (2013). Truss-arch model for shear strength of shear-critical reinforced concrete columns. *Journal of Structural Engineering, 139*(4), 548–560.

Pan, Z., Li, B., & Lu, Z. (2014). Effective shear stiffness of diagonally cracked reinforced concrete beams. *Engineering Structures, 59*(2), 95–103.

Pan, Z., Wu, C., Liu, J. W., et al. (2015). Study on mechanical properties of cost-effective polyvinyl alcohol engineered cementitious composites (PVA-ECC). *Construction and Building Materials, 78*(3), 397–404.

Paulay, T., & Priestley, M. J. N. (1992). *Seismic design of reinforced concrete masonry buildings*. New York: Wiley.

Schlaich, J., Schäfer, K., & Jennewein, M. (1987). Toward a consistent design of structural concrete. *PCI Journal, 32*(3), 74–150.

Won, P. S., & Vecchio, F. J. (2002). VecTor2 & form works user's manual [EB/OL]. <http://www.civ.utoronto.ca/vector/>.

Wu, C., Pan, Z., Su, R. K. L., Leung, C. K. Y., & Meng, S. (2017). Seismic behavior of steel reinforced ECC columns under constant axial loading and reversed cyclic lateral loading. *Materials and Structures, 50*(1), 78.

Yoo, D. Y., & Yoon, Y. S. (2016). A review on structural behavior, design, and application of ultra-high-performance fiber-reinforced concrete. *International Journal of Concrete Structures and Materials, 10*(2), 125–142.